A CFD and experimental investigation into a non-intrusive method for measuring cooling air mass flow rate through a synchronous generator

K Bersch[1], P H Connor[1], C N Eastwick[1], M Galea[2 3]

[1]*Fluids and Thermal Engineering Research Group, Faculty of Engineering, University of Nottingham, Nottingham, UK,*

kevin.bersch@nottingham.ac.uk, peter.connor@nottingham.ac.uk, carol.eastwick@nottingham.ac.uk

[2]*Power Electronics, Machines and Control Research Group, Faculty of Engineering, University of Nottingham, Nottingham, UK, michael.galea@nottingham.ac.uk*

[3]*Power Electronics, Machines and Control Research Group, Faculty of Engineering, University of Nottingham Ningbo China, Ningbo, China*

Keywords: CFD, Design, Electrical Machine, Experimental Validation, Thermal Management

Abstract

This paper presents a detailed methodology for a non-intrusive measurement of cooling air mass flow rate that enables an overall machine evaluation. This approach enables the simultaneous measurement of air mass flow with shaft torque at differing operating points, while minimising the change in air flow introduced by the measurement system. The impact of geometric parameters in the designed system are investigated using a detailed 180° CFD model. Special attention was paid to minimising their influence on pressure drop, mass flow rate through the machine and measurement uncertainty. Based on the results of this investigation, the system was designed and manufactured and the experimentally measured data was used to validate the CFD predictions. For the as optimal identified configuration, the flow rate is predicted to decrease by 2.2 % relative to unrestricted operation. The achieved measurement uncertainty is ±2.6 % at synchronous speed.

1 Introduction

Appropriate cooling of electrical machines is important to maximise efficiency [1] and ensure safe and long term operation [2]. Small to medium sized synchronous generators are often cooled by air being driven through the machine core by a fan. The average and peak winding temperatures are directly related to the air mass flow rate, making it an important characteristic in determining the cooling performance. Furthermore, the flow rate influences local flow velocities, which are widely used as an input parameter for lumped parameter thermal network (LPTN) models [3], [4]. The mass flow rate is also used for the validation of CFD models created to predict the thermal behaviour of the machine [5]–[7]. Therefore it is essential to accurately determine the air mass flow rate under normal operating conditions.

Conventional testing approaches for airflow on electrical machines often involve the use of vane or hot wire anemometers at the machine inlets or outlets. But these measurements are fraught with a variety of uncertainties. Generally, the velocity profiles over the inlets and outlets vary locally, making it difficult to determine an average velocity to calculate the mass flow rate. The anemometer needs to be perfectly aligned with the flow direction to measure the velocity correctly. Additionally, the measurement might influence the measured flow rate by blocking the flow path, particularly if a vane anemometer is used on a small machine.

Another possible approach is to cover the machine inlets or outlets directly with a duct and measure the flow rate inside the duct. The flow rate measurement can be taken using anemometers or air flow sensors [8], eliminating the problem of locally varying velocities described previously. Alternatively, a calibrated inlet duct for which the correlation between the pressure drop in a specific location and mass flow rate is known can be used [7], [9]. While this approach is more accurate than manual measurements using handheld anemometers, it can change the inflow considerably in comparison to unrestricted operation. Thus the measured flow rate could be different from the one at normal operation.

Surrounding the alternator with a sufficiently large, airtight box, or plenum, and connecting its only opening to a duct to measure the flow rate can be a much more accurate method (view Figure 1). This approach enables highly accurate measurements using well-understood pipe flow correlations while minimising the change in inflow and outflow conditions if the system is designed correctly. This method has been used successfully by other authors in the past [5].

The novelty in this paper is the detailed analysis of the complex, inter-dependent system behaviour of the machine, plenum and inlet duct. The optimisation of their sizing is a

balance between resulting physical changes in the inflow conditions introduced by the measurement method and measurement accuracy. Reducing the duct diameter enables a higher measurement accuracy as the duct velocity, and following the measurable drop in static pressure in the duct, increases. But the added pressure drop, that needs to be overcome by the fan, causes a reduction in flow rate compared to unrestricted operation. Choosing a larger duct diameter reduces the change in inflow conditions at the cost of measurement accuracy.

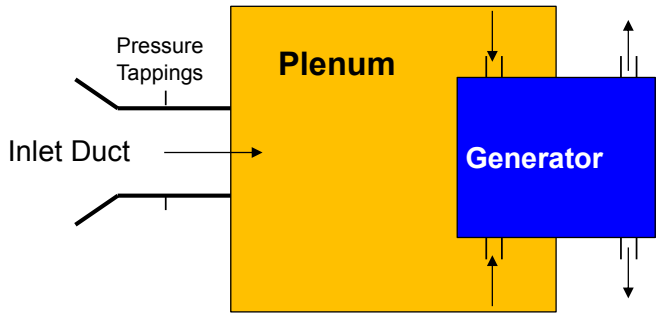

Figure 1: Schematic of presented non-intrusive measurement technique

2 Methodology

2.1 CFD Investigations

The CFD investigations were performed using ANSYS Fluent within ANSYS Workbench 17.2. A complex 180° model of a generator's internal rotating flow, as well as external airflow regions, has been created to predict the flow rate through the machine. The plenum and duct dimensions were parameterised, enabling the user to analyse the air flow properties around and through the generator for different system configurations. Machine and plenum are surrounded by a large cylindrical domain to ensure the domain boundaries are sufficiently far away from the zone of interest to not interfere with the flow solution. The domain boundaries are defined as walls. Figure 2 shows the geometry created in ANSYS Designmodeler.

The investigated machine possesses two inlets at the Drive End and four outlets at the Non Drive End, which are covered with grilles for health and safety reasons. Modelling the flow through the grilles correctly would require a very fine mesh in this region and would therefore be computationally expensive. For that reason, the grilles were neglected in the CFD model and removed from the machine for validation purposes during the experimental testing.

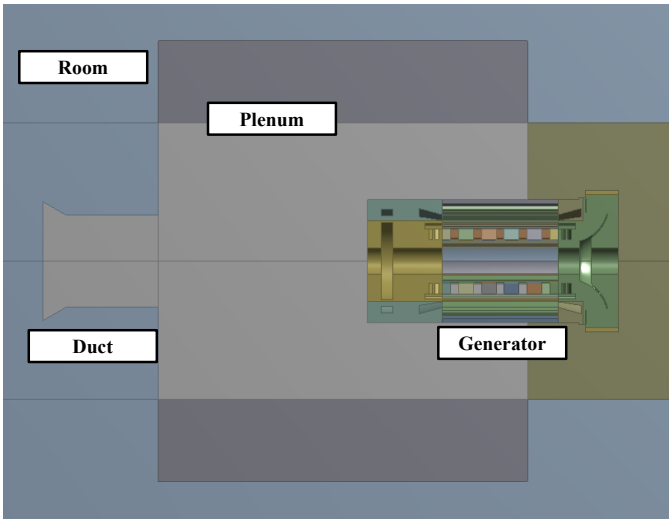

Figure 2: CFD geometry used to determine the optimal plenum and duct dimensions

The standard k-ε model with Enhanced Wall Treatment was chosen for turbulence modelling due to its robustness and the possibility to use wall functions instead of having to resolve the boundary layer for all walls. It is commonly used for radial flux machines and has been validated for them by a number of researchers [6], [7], [10]–[12]. Pressure and velocity were coupled by the SIMPLE algorithm. The spatial discretisation of all variables is second order accurate.

Rotation is modelled using the Multiple Reference Frame (MRF) technique. While the flow inside a generator is transient, this approach allows the case to be simulated as steady-state with respect to the moving frame. The moving parts are frozen in a specific location and the flow field developing in that position can be observed [13]. While less accurate than using the fully transient Sliding Mesh (SM) approach, it is normally used for the analysis of electrical machines [6], [7], [10]–[12], [14] due to the much lower computational effort required.

2.2 Experimental validation

2.2.1. Mass flow test setup

The duct and plenum were manufactured to the optimal dimensions identified by the CFD investigations (view section 3). The plenum is built out of 9 mm plywood supported by a timber framework and can be assembled and disassembled easily due to its modular construction. To enable access to the generator while the plenum is in place, a door was added next to the inlet duct opening. Air tightness was ensured by sealing the gaps between adjacent plywood sheets with silicone or duct tape. Figure 3 shows the assembled plenum and inlet duct in the lab environment.

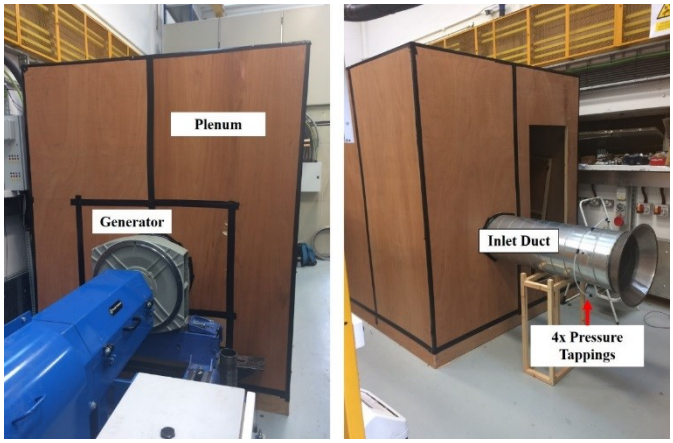

Figure 3: Manufactured plenum; Front view (left); Back View including conical inlet duct (right)

The duct is manufactured according to B.S.848[15] featuring a conical inlet and four static pressure tappings located equidistant circumferentially downstream of the inlet. They are connected together with plastic tubing. A "Sensocon A1 Digital Differential Pressure Gauge" is used to measure the averaged pressure drop over the four tappings. The mass flow rate ṁ can be calculated from the pressure drop Δp using the following correlation provided in [15]:

$$\dot{m} = \alpha\varepsilon\pi\frac{d_d^2}{4}\sqrt{2\rho\Delta p} \qquad (1)$$

The compound coefficient αε is dependent on the duct Reynolds number and amounts to 0.94 for this application. d_d is the inner diameter of the inlet duct. ρ is the air density upstream of the conical inlet and has been determined by measuring the air temperature close to the inlet with a PT100 RTD.

Mass flow measurements were taken at 150 RPM intervals from 450-1500 RPM. Below that, the uncertainty of the pressure gauge is not sufficient to provide useful data. The pressure measurements were logged with a frequency of 5 Hz and averaged over a timeframe of at least one minute. Even though the flow rate changes pretty much instantaneously with the change of rotational speed, the machine was run at each speed for at least one minute before collecting the data to be averaged.

2.2.2. Torque test setup

An 'HBM T12 Torque Transducer', located between the drive motor and the coupling, was used to determine the no load torque. It can measure torque from 0-10 kNm with a 0.03 % full scale accuracy. The collected data was measured with a sampling rate of 300 Hz and logged via a "HBM QuantumX data acquisition system" connected to the torque transducer.

For the first two hours of operation, the torque decreases steadily. This is mainly caused by the warming up of the grease in the bearings, decreasing its viscosity thus reducing friction. Therefore all torque tests have been performed after warming up the machine for at least two hours.

The measured torque includes the bearing friction torque M_B, which is not included in the CFD model. Hence it needs to be subtracted from the measurements for validation purposes. It can be estimated from the bearing friction coefficient μ, the radial load of the bearing F_R and the bearing bore diameter d_B using the following correlation:

$$M_B = 0.5\mu F_r d_B \qquad (2)$$

Torque measurements were taken at 150 RPM intervals from 150-1500 RPM. After the initial warmup period, the rig was stopped and the torque transducer zeroed. The speed was then increased (initially to 1500 RPM) and held constant for 20 minutes. This procedure was repeated for the subsequent measurements with decreased speed. A slight drop in torque was observed over the first few minutes after every speed change. Therefore the torque data was averaged over the steady value recorded over the last 10 minutes of each operating point.

3 Results and Discussion

3.1 CFD results

The flow rate through the machine is dependent on the pressure drop the fan needs to overcome. As the duct and plenum reduce the air pressure at the generator inlet, the CFD results can be used to predict the reduction in mass flow rate when compared to unrestricted operation. In Figure 4, the static pressure drop introduced by the measurement system can clearly be seen.

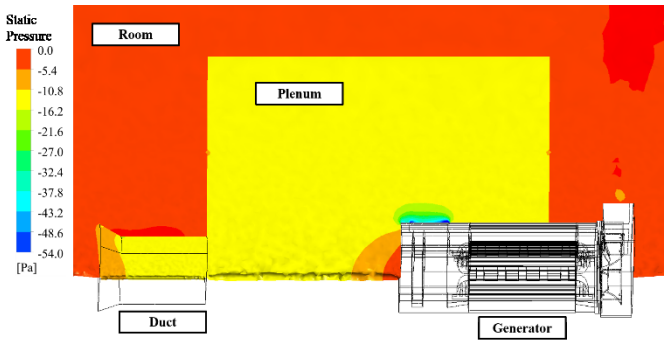

Figure 4: CFD prediction of static pressure drop introduced through plenum and duct

The increased pressure drop is caused by the following factors:

Contraction/Expansion at the duct inlet/outlet
The contraction at the duct inlet and the sudden expansion at the outlet cause energy to be dissipated resulting in an irreversible pressure drop.

Friction and turbulent energy dissipation
Kinetic energy is converted to heat due to internal fluid friction, wall friction and turbulent dissipation resulting in an irreversible pressure drop.

Conversion of static pressure to kinetic energy in the duct
The increase in flow velocity in the duct causes the static pressure to drop resulting in a reversible pressure drop. Most of the kinetic energy cannot be recovered in this configuration however, as the majority of the flow impinges onto the

generator back plate after exiting the duct. Placing a flow deflector between duct and generator would decrease the pressure drop, but was considered unnecessary for this application, as the change in flow rate of the optimal system configuration is small enough to be considered negligible. Figure 5 shows that the flow into the machine with the measurement system in place is very similar to unrestricted operation.

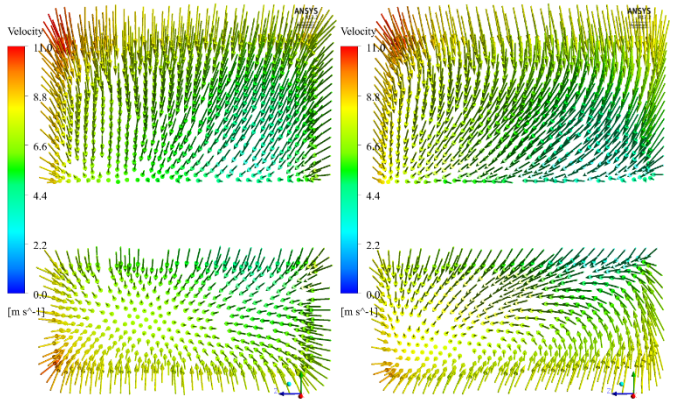

Figure 5: Comparison of the velocity vectors at the machine inlet; Unrestricted (left); Plenum with 400 mm duct (right)

Initially, a model without the plenum system was solved to provide baseline data against which the influence of the measurement system could be compared. Table 1 gives an overview over various simulated duct and plenum configurations and the influence they have on key parameters of interest, such as the change in mass flow rate and measurement uncertainty.

Duct diameter (mm)	**Plenum dimensions (m)**	**Added Pressure Drop (Pa)**	**Change in flow rate**	**Measure-ment uncertainty**
200	**1x1x1**	148	-19.9 %	0.2 %
300	**1x1x1**	51	-6.2 %	0.9 %
100	**1.9x1.5x1.6**	337	-69.4 %	0.1 %
150	**1.9x1.5x1.6**	247	-40.3 %	0.1 %
200	**1.9x1.5x1.6**	148	-18.7 %	0.2 %
250	**1.9x1.5x1.6**	81	-9.5 %	0.5 %
300	**1.9x1.5x1.6**	47	-5.7 %	0.9 %
400	**1.9x1.5x1.6**	16	-2.2 %	2.6 %
500	**1.9x1.5x1.6**	8	-1.1 %	6.2 %

Table 1: Comparison of added pressure drop and change in mass flow rate for various plenum and duct configurations

The added pressure drop at the machine inlet increases with decreasing duct diameter and plenum dimensions, reducing the flow rate. Especially the duct diameter impacts the flow rate considerably. Figure 6 shows how the flow rate through the generator changes with the duct diameter for a constant plenum size of 1.9 m x 1.5 m x 1.6 m. The mass flow rate has been normalised according to the following equation:

$$\dot{m}_n = \frac{\dot{m}}{\dot{m}_u} \quad (3)$$

with ṁ being the mass flow rate for the specific duct diameter and $\dot{m}_u$ the flow rate for the unrestricted case.

The duct diameter determines the magnitude of the static pressure measured in the duct pressure tappings. Rearranging Equation (1) shows that the pressure drop, which is used to calculate the mass flow rate, is inversely proportional to the fourth power of the duct diameter. As the measurement uncertainty of the used pressure gauge is constant over the full pressure range, the mass flow rate measurement uncertainty $\pm\dot{m}$ increases with the duct diameter as following:

$$\pm\dot{m} \sim d_d^4 \quad (4)$$

As a result of the CFD investigations, it was decided to use a 400 mm duct. It enables a reasonable measurement uncertainty for 30-100 % synchronous speed while decreasing the flow rate by only 2.2 %. The dimensions of the manufactured plenum were chosen as 2.44 m x 2.00 m x 2.00 m, utilising all the available space around the test rig.

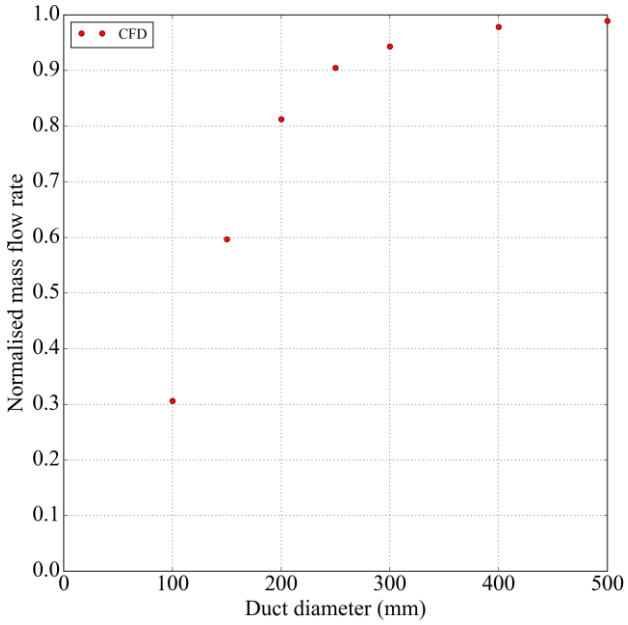

Figure 6: Correlation between duct diameter and normalised mass flow rate predicted by CFD for a plenum size of 1.9 m x 1.5 m x 1.6 m

3.2 Mass flow validation

In Figure 7, CFD and experimental mass flow rates at different rotational speeds are compared. The experimental measurements were taken without grilles covering the inlets and outlets. CFD and experimental results show reasonable agreement. The trend is predicted correctly. The maximum difference between CFD and experimental data amounts to 13 % at synchronous speed.

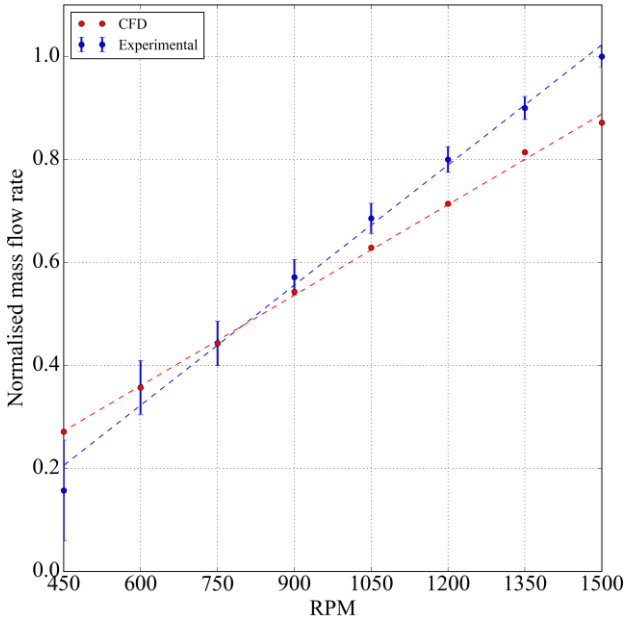

Figure 7: Comparison of CFD and experimental mass flow measurements

3.3 Torque validation

Figure 8 shows a comparison of CFD torque and experimental data at various rotational speeds. The bearing friction torque, calculated according to Equation (2), was subtracted from the experimental results, as the bearings are not considered in the CFD model.

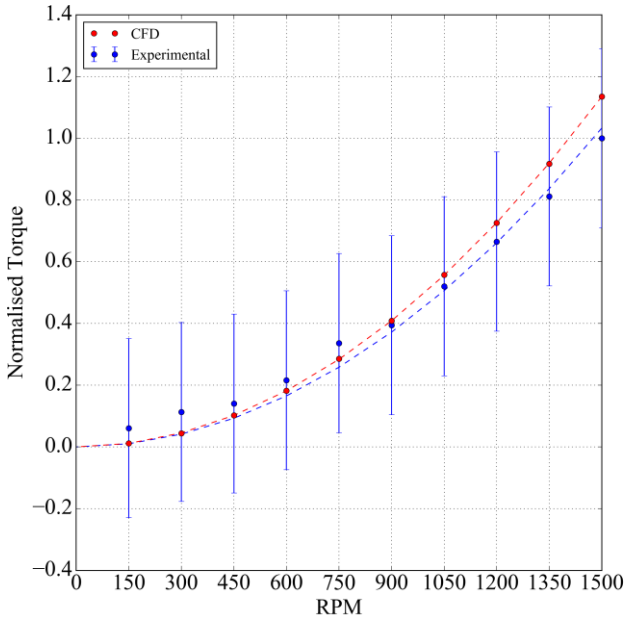

Figure 8: Comparison of CFD and experimental torque measurements

CFD and experimental results show good agreement. The trend is predicted correctly. The maximum difference between CFD and experimental data amounts to 16 % at synchronous speed. As the utilised torque transducer is used for measuring torque and controlling the rig at full load, its accuracy at no load is relatively poor. In future work, these measurements will be repeated with a more accurate torque transducer.

4 Conclusion

A non-intrusive measurement method of cooling air mass flow rate through a synchronous generator has been designed using CFD. Special attention has been paid to determining the optimal dimensions of the measurement duct and plenum, minimising the change in flow rate in comparison to unrestricted operation while maintaining a sufficient measurement accuracy. For the as optimal identified configuration, the flow rate is predicted to decrease by 2.2 % relative to unrestricted operation. The achieved measurement uncertainty is ±2.6 % at synchronous speed. The system was manufactured according to the results of the CFD simulations and the experimental data shows good agreement with the flow rate and torque predicted by CFD validating the design methodology.

Acknowledgements

The authors would like to thank the Power Electronics, Machines and Control Group technical staff for their support.

References

[1] A. Boglietti, A. Cavagnino, D. Staton, M. Shanel, M. Mueller, and C. Mejuto, “Evolution and Modern Approaches for Thermal Analysis of Electrical Machines,” *IEEE Trans. Ind. Electron.*, vol. 45, 2009.

[2] J. Pyrhönen, T. Jokinen, and J. Hrabovcová, *Design of rotating electrical machines*. Chichester, 2014.

[3] D. A. Staton and A. Cavagnino, “Convection heat transfer and flow calculations suitable for electric machines thermal models,” *IEEE Trans. Ind. Electron.*, vol. 55, no. 10, pp. 3509–3516, 2008.

[4] D. Staton, A. Boglietti, and A. Cavagnino, “Solving the more difficult aspects of electric motor thermal analysis in small and medium size industrial induction motors,” *IEEE Trans. Energy Convers.*, vol. 20, no. 3, pp. 620–628, 2005.

[5] P. H. Connor, S. J. Pickering, C. Gerada, C. N. Eastwick, C. Micallef, and C. Tighe, “Computational fluid dynamics modelling of an entire synchronous generator for improved thermal management,” *IET Electr. Power Appl.*, vol. 7, no. 3, pp. 231–236, 2013.

[6] P. H. Connor, “Computational Fluid Dynamics Modelling of a Synchronous Electric Generator,” University of Nottingham, 2014.

[7] M. Shanel, “Investigation of Rotor Cooling in Salient

Pole Electrical Machines," University of Nottingham, 2002.

[8] A. S. Fawzal, R. M. Cirstea, K. N. Gyftakis, T. J. Woolmer, M. Dickison, and M. Blundell, "The Fan Design Impact on the Rotor Cooling of Axial Flux Permanent Magnet Machines," *ICEM 2016*, pp. 2727–2733, 2016.

[9] D. A. Howey, "Thermal design of air-cooled axial flux permanent magnet machines," Imperial College London, 2010.

[10] C. Micallef, "End winding cooling in Electric Machines," University of Nottingham, 2006.

[11] S. J. Pickering, D. Lampard, J. Mugglestone, and M. Shanel, "Using CFD in the Design of Electric Motors and Generators," *Comput. Fluid Dyn. Pract.*, 2001.

[12] J. Mugglestone, D. Lampard, and S. J. Pickering, "Effects of end winding porosity upon the flow field and ventilation losses in the end region of TEFC induction machines," *IEE Proc. Electr. Power Appl.*, vol. 145, no. 5, pp. 423–428, 1998.

[13] Fluent, "ANSYS FLUENT User's Guide v17.2," 2016.

[14] K. Bersch, P. H. Connor, C. N. Eastwick, M. Galea, and R. Rolston, "CFD Optimisation of the Thermal Design for a Vented Electrical Machine," in *Proceedings - 2017 IEEE Workshop on Electrical Machines Design, Control and Diagnosis, WEMDCD 2017*, 2017, pp. 39–44.

[15] British Standard, "Industrial fans — Performance testing using standardized airways," vol. 3, no. May, 2009.